



A 350,000-year-old blue ice identified at the surface of the Elephant Moraine region, East Antarctica

Giyeon Lee¹, Jinho Ahn^{1*}, Hyeontae Ju², Ikumi Oyabu^{3,4}, Florian Ritterbusch⁵, Songyi Kim⁶, Jangil Moon⁶, Joohan Lee², Yeongcheol Han⁶, Soon Do Hur⁶, Kenji Kawamura^{3,4,7}, Zheng-Tian Lu^{5,8}, Wei Jiang^{5,8} and Guo-Min Yang^{5,8}

¹School of Earth and Environmental Sciences, Seoul National University, Seoul, 08826, South Korea

²Center of Technology Development, Korea Polar Research Institute, Incheon, 21990, South Korea

³National Institute of Polar Research, Research Organization of Information and Systems, Tachikawa, 190-8518, Japan

⁴Polar Science Program, Graduate Institute for Advanced Studies (SOKENDAI), Tachikawa, 190-8518, Japan

10 ⁵Hefei National Research Center for Physical Sciences at the Microscale and School of Physical Sciences, University of Science and Technology of China, Hefei, 230026, China

⁶Division of Glacier & Earth Sciences, Korea Polar Research Institute, Incheon, 21990, South Korea

⁷Japan Agency for Marine-Earth Science and Technology (JAMSTEC), Yokosuka, 237-0061, Japan

⁸Hefei National Laboratory, University of Science and Technology of China, Hefei, 230088, China

15 *Correspondence to:* Jinho Ahn (jinhoahn@snu.ac.kr)

Abstract. For addressing important paleoclimatic questions, such as the cause of the Mid-Pleistocene Transition (MPT), the search for one-million-year-old ice is of great interest. Antarctic blue-ice areas (BIAs), where ancient ice outcrops on the surface of ice sheet, offer promising sites for identifying ice spanning the MPT period. To date, only two sites, the Allan Hills BIA and the Mullins Glacier in East Antarctica, have been identified as areas that contain ancient ice older than one million years. We investigated icefields in the Elephant Moraine and Reckling Moraine regions of East Antarctica to contribute to the search for ancient ice spanning the MPT. Ice-penetrating radar surveys revealed that ice thickness ranged from 200 m to 800 m across the icefields. The ⁸¹Kr dating of the surface ice (<10 m) showed ages of 83–119 kyr BP (Before Present) and 93–124 kyr BP for blue ice in the Meteorite City Icefield and 320–385 kyr BP in the Elephant Moraine Main Icefield. We also analyzed several gas compositions ($\delta^{15}\text{N-N}_2$, $\delta^{18}\text{O-O}_2$, $\delta\text{O}_2/\text{N}_2$, $\delta\text{Ar}/\text{N}_2$, CO_2 , CH_4 , and N_2O) and revealed that gas records at very shallow depths are altered. A comparison of stable water isotopes ($\delta^{18}\text{O}_{\text{ice}}$ and $\delta^2\text{H}_{\text{ice}}$) indicated that the original deposition site of the Elephant Moraine Main Icefield experienced colder condition than those of the nearby icefields. Given these findings, we expect that ice spanning the MPT period can be retrieved from the Elephant Moraine Main Icefield with only a few hundred meters of drilling.



1 Introduction

30 Glacial ice in the polar ice sheets is formed by the compaction of accumulated snow. During this densification process, the air in the firn becomes gradually isolated and trapped as bubbles within the ice, thereby serving as an invaluable archive of ancient atmospheric air (Schwander and Stauffer, 1984). Glacial ice then flows toward the margins of the ice sheet under the influence of gravity. When it encounters topographic obstacles such as nunataks, the ice flow is redirected and thereafter outcrops at the surface of the ice sheet in so-called blue-ice areas (BIAs) (Bintanja, 1999; Sinisalo and Moore, 2010; Gardner et al., 2018). Ice layers of the same age are extended to the surface of the BIAs. As a result, virtually unlimited amounts of ancient ice of specific ages can be obtained cost-effectively in BIAs compared to conventional deep-ice-core-drilling projects.

The 800,000-year-old EPICA Dome C (EDC) ice core, the oldest continuous ice core, has contributed significantly to past atmospheric air composition reconstructions and enhanced our understanding of the Earth's climate system (EPICA community members, 2004; Louergue et al., 2008; Extier et al., 2018). Nevertheless, to address important questions—such as the cause of the Mid-Pleistocene Transition (MPT), when glacial-interglacial cycles changed from a 40,000-year to a 100,000-year cycle approximately one million years ago—ongoing efforts aim to retrieve ice cores older than one million years (Fischer et al., 2013; Lilien et al. 2021). Shallow ice core drilling in BIAs has also been conducted as part of this initiative.

The total area of BIAs in Antarctica is estimated to be 234,549 km², accounting for approximately 1.67 % of the Antarctic continent (Hui et al., 2014). Several BIAs have been dated using various methods such as ice flow modeling, radiometric analysis, and the synchronization of glaciochemical and/or gas records with well-dated ice cores (Moore et al., 2006; Dunbar et al., 2008; Lee et al., 2022; Hu et al., 2024). The estimated age of ice in Antarctic BIAs range from thousands to millions of years (Table 1). The oldest ice is found in the Allan Hills BIA, where the surface ice age ranges from 90 kyr BP to 250 kyr BP (Before Present) (Spaulding et al., 2013), and ice at depths of 200 m dates back to approximately 6 Myr BP (Higgins et al., 2025). Although the ice stratigraphy in the Allan Hills BIA is substantially disordered, it has provided snapshots of past atmospheric oxygen and greenhouse gas (GHG) variations from the pre-MPT period (Yan et al., 2019; Yan et al., 2021). Ice at depths of 3–32 m from the Mullins Glacier has also been dated to the pre-MPT period (Table 1) (Yau et al., 2015). However, pristine gas records suitable for paleoclimatic reconstruction are missing in Mullins Glacier (Yau et al., 2015). To better understand the causes of the MPT, it is essential to obtain an ice core continuously spanning this period with pristine gas records. Based on the discovery of pre-MPT ice in the Allan Hills BIA and Mullins Glacier, Antarctic BIAs may provide promising sites for recovering such an ice core by shallow drilling. To identify potential sites, chronological studies of the surface ice in BIAs must first be conducted.

In this study, we investigated icefields in the Elephant Moraine (EM) and Reckling Moraine (RM) regions, focusing primarily on constraining the age of blue ice in the EM region. We first began with assessing the bedrock topography and ice thickness using ice-penetrating radar (IPR) surveys. Next, we took the measurements of trapped air (e.g. ⁸¹Kr, ⁸⁵Kr, $\delta^{15}\text{N-N}_2$, $\delta^{18}\text{O-O}_2$, $\delta\text{O}_2/\text{N}_2$, $\delta\text{Ar}/\text{N}_2$, CO_2 , CH_4 , and N_2O) in EM blue ice and stable water isotopes ($\delta^{18}\text{O}_{\text{ice}}$ and $\delta^2\text{H}_{\text{ice}}$) of the RM and EM



blue ice. Finally, considering potential alterations in the measured gas components, we determined the age of the EM blue ice through ^{81}Kr dating and chemical analyses of the trapped air.

Table 1. Age constraints of Antarctic blue-ice areas (BIAs).

Blue-ice areas	Age (kyr BP)	Location	References
Elephant Moraine	101, 108, 351	76.27° S, 156.71° E	This study
Allan Hills	90–250, 2700, 6000	76.73° S, 159.36° E	Spaulding et al. (2013), Yan et al. (2019), Higgins et al. (2025)
Frontier Mountain	<50	72.98° S, 160.33° E	Folco et al. (2006)
Grove Mountains	143	72.99° S, 75.22° E	Hu et al. (2024)
Larsen Glacier	6–25	74.93° S, 161.60° E	Lee et al. (2022)
Mt. Moulton	105–136, 496	76.67° S, 134.70° W	Dunbar et al. (2008), Korotkikh et al. (2011)
Mullins Glacier	1600	77.88° S, 160.54° E	Yau et al. (2015)
Nansen	<130	72.75° S, 24.50° E	Zekollari et al. (2019)
Patriot Hills	1–80, 130–134	80.30° S, 81.35° W	Turney et al. (2020)
Scharffenbergbotnen	<11	74.56° S, 11.05° W	Sinisalo et al. (2007)
South Yamato	55–61	72.08° S, 35.18° E	Moore et al. (2006)
Taylor glacier	9–133	77.75° S, 161.80° E	Buizert et al. (2014)

2 Study area and methods

65 2.1 Study area

During the 2016/17 austral summer, shallow ice cores (5–10 m in length) were collected from the icefields within the EM region (Fig. 1) (Jang et al., 2017). Additionally, during the 2018/19 austral summer, 70 surface ice samples (5–10 cm depth) were collected along a 700 m transect at 10 m intervals from the icefield in the RM region (Fig. 1).

The EM and RM regions are renowned as Antarctic meteorite stranding zones (Cassidy et al., 1992). The EM region consists of several distinct icefields: the Northern Ice Patch, Meteorite City Icefield, Texas Bowl Icefield, and the Elephant Moraine Main Icefield (Fig. 1) (Righter et al., 2021). The tephra layer observed in the Meteorite City Icefield (76.25°S, 156.56°E) indicate that the dip of the ice layers range from 20° to 60° (Jang et al., 2017). The mean annual temperature in the EM region is -30.3°C (Lee et al., 2022), and the annual ablation rate is estimated at $4.1 \pm 0.1 \text{ cm yr}^{-1}$, with a slightly higher rate of $4.7 \pm 0.2 \text{ cm yr}^{-1}$ at RM (Faure and Buchanan, 1991). Ice flows from southwest to northeast at a speed of approximately $1\text{--}5 \text{ m yr}^{-1}$ (Rignot et al., 2011; Mouginot et al., 2012) (Fig. 1).

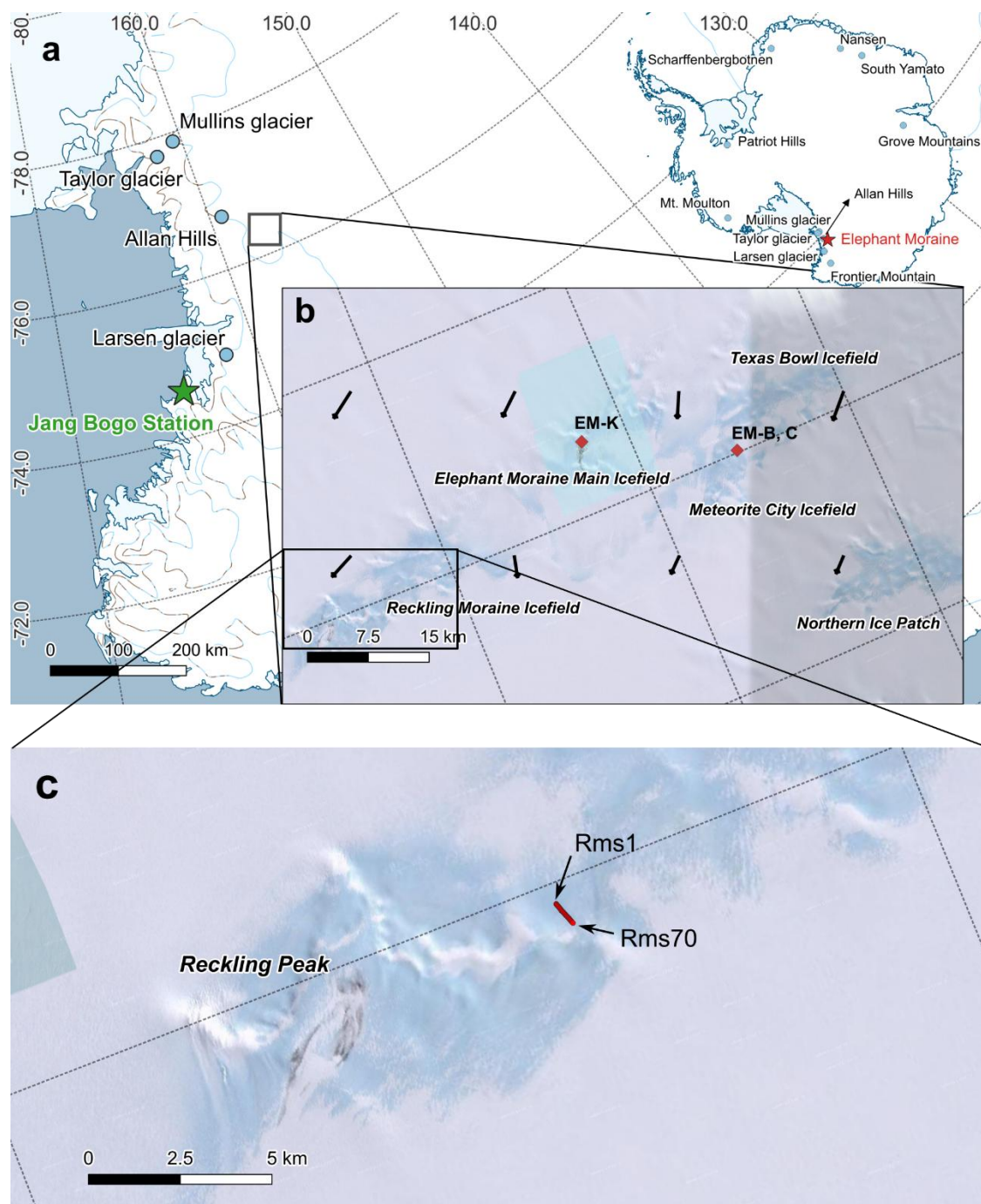


Figure 1. Map of Elephant and Reckling Moraine regions. (a) The area of Victoria Land, East Antarctica and sites of BIAs. (b) Magnified area, including sampling locations of ice core (red diamond). Arrows show the ice flow direction. (c) Magnified area, including sampling locations of surface ice (red circles). The map was made using the QGIS Quantarctica package with a satellite image from © Google Earth (Rignot et al., 2011; Mouginot et al., 2012).

2.2 Ice-Penetrating Radar (IPR) survey

During the 2018/19 austral summer, an ice-penetrating radar (IPR) survey was conducted across the EM and part of the RM region to estimate the bedrock elevation and ice thickness. The survey was performed using airborne IPR with 5 km grid spacing, covering a total distance of 384 km. The Helicopter-borne Radar (HERA) system, developed by the University of Texas Institute for Geophysics, was mounted inside a helicopter with two radar boom antennas. The helicopter maintained a constant operating speed of approximately 36 m s^{-1} throughout the survey. Data were recorded at 3200 samples per trace, with a 20 ns sampling interval and a total recording time of 64 μs . The x-axis resolution was approximately 9 m per trace, and the y-axis resolution was approximately 1.69 m per sample.

The surface elevation (z_s) of the ice was calculated by subtracting the flight height above the surface (h_l), measured using a laser altimeter, from the flight altitude (z_{hf}), recorded by the Global Navigation Satellite System (GNSS) onboard the helicopter (Eq. (1)). The ice thickness (h_{ice}) was determined by identifying the air-ice and ice-bedrock interfaces in the radar profiles and multiplying the two-way travel time by the radar wave velocity in ice ($v_{ice} = 0.169 \text{ m ns}^{-1}$, Reynolds, 2011). The bedrock elevation (z_{bed}) was estimated by subtracting the ice thickness from the surface elevation (Eq. (2)). The bedrock elevation and ice thickness between survey lines were interpolated using the Kriging method.

$$z_s = z_{hf} - h_l \quad (1)$$

$$z_{bed} = z_s - h_{ice} \quad (2)$$

2.3 ^{81}Kr dating

For ^{81}Kr dating, 6–10 kg of ice was used for each measurement (Table 2). Because of ice core availability, we mixed different depth ranges for EM-B and EM-K (Table 2). Trapped air was extracted using an ice melter described by Tian et al. (2019). The ice samples were placed in a stainless-steel tank, which was pre-evacuated using a dry scroll pump equipped with a water trap. The ice was then melted by immersing the tank in hot water to release the trapped gas. The extracted gas was collected in a stainless-steel container and transported to the University of Science and Technology of China (USTC) for Kr purification and ^{81}Kr analysis. ^{81}Kr analysis was performed using the Atom Trap Trace Analysis (ATTA) method. ^{85}Kr was also measured to quantify the potential contamination from modern air. The details about the extraction procedure and the ATTA method can be found in Tian et al. (2019) and Jiang et al. (2012).

Table 2. Results of Kr analysis of shallow ice cores from Elephant Moraine region. TAC: total air content, STP: standard temperature and pressure, dpm cm^{-3} : decay per minute per cubic centimeter of Kr, pMKr: percent modern krypton.

Sample	Extracted air (mL)	Mass (kg)	TAC ($\text{cm}^3 \text{ STP g}^{-1}$)	Depth (cm)	^{85}Kr (dpm cm^{-3})	^{81}Kr (pMKr)	^{81}Kr age (kyr BP)	Systematic error (kyr)
--------	--------------------	-----------	--	------------	--	-------------------------	-------------------------------	------------------------



EM-B	432	9.3	0.043	515–762.5, 795.5–967.5	<1.0	74.1 ± 3.9	101 ⁺¹⁷ ₋₁₇	± 4.9
EM-C	517	10.1	0.048	271.5–680.5	<0.8	72.4 ± 3.3	108 ⁺¹⁵ ₋₁₄	± 5.2
EM-K	425	6.4	0.061	151–283.5, 329.5–384.5, 464.5–568	5.2 ± 0.4	39.0 ± 2.6	351 ⁺²⁹ ₋₂₆	± 16.9
Air in Seoul (Nov. 2019)	-	-	-	-	78.9 ± 1.9	-	-	-

2.4 $\delta^{15}\text{N-N}_2$, $\delta^{18}\text{O-O}_2$, $\delta\text{O}_2/\text{N}_2$, and $\delta\text{Ar/N}_2$

Six ice samples were cut from the EM ice cores and sent to the National Institute of Polar Research (NIPR) in Japan for the simultaneous measurement of O_2 , N_2 , and Ar isotopes using a dual-inlet mass spectrometer (Thermo Fisher Delta V). The outermost surface and any large cracks were carefully trimmed by approximately 3–5 mm, and blurry ice surfaces were shaved off using a ceramic knife. The final mass of the sample was 70–130 g. The ice was then loaded into a stainless-steel vessel, and the trapped gas was released by immersing it in hot water. The released gas was cryopumped, passed through a water trap, and finally collected in a stainless-steel tube for analysis. Further details on the extraction procedure can be found in the study by Oyabu et al. (2020).

The isotope ratios of gases in ice cores can be affected by fractionation owing to gravitational settling and thermal diffusion in the firn column (Craig et al., 1988; Severinghaus et al., 1998; Goujon et al., 2003). To correct for gravitational fractionation, we applied Eq. (3).

$$\delta_{\text{grav}} = \delta_{\text{measured}} - (\Delta m \times \delta^{15}\text{N}) \quad (3)$$

Δm represents the mass difference between heavy and light isotopes; 2 for $\delta^{18}\text{O-O}_2$ ($^{18}\text{O}/^{16}\text{O}$), 4 for $\delta\text{O}_2/\text{N}_2$ ($^{32}\text{O}_2/^{28}\text{N}_2$), and 12 for $\delta\text{Ar/N}_2$ ($^{40}\text{Ar}/^{28}\text{N}_2$). We assumed that thermal fractionation correction was not necessary because the relatively gradual climate change in Antarctica is unlikely to induce a significant temperature gradient within the firn column (Severinghaus et al., 1998; Goujon et al., 2003).

Gas loss can occur due to storage temperatures above -50°C and/or the presence of numerous fractures in the ice, leading to depletion in $\delta\text{O}_2/\text{N}_2$ values and enrichment in $\delta^{18}\text{O-O}_2$ values in bubbly ice (Bender et al., 1995; Ikeda-Fukazawa et al., 2005; Severinghaus et al., 2009). However, due to insufficient measurements for gas loss correction, we could not apply gas loss correction in this study (Landais et al., 2003; Capron et al., 2010). The final isotope ratios are reported relative to those in the modern atmosphere.



2.5 Greenhouse gas concentrations (CO₂, CH₄, and N₂O)

130 The CO₂ concentrations in the EM blue ice (EM-B, EM-C, and EM-K) were measured at SNU. To eliminate potential contamination from ambient air, the outermost surface and large cracks of the ice were carefully trimmed to approximately 1–2 mm using a band saw. Ice (15–20 g) was then placed in a double-walled vacuum chamber maintained at –35 °C during sample preparation. The trapped ancient air within the ice was released using a needle crusher, cryopumped through a –85 °C water trap, and finally condensed in stainless-steel tubes at 12 K (–261 °C). The tubes were then warmed up in hot water and
135 attached to a flame ionization detector gas chromatograph (FID-GC) to measure the CO₂ concentration. Because of the limited amount of CO₂, we used a Ni-catalyst to convert it into CH₄ before reaching the detector, which increased the sensitivity (Ahn et al., 2009; Shin et al., 2022). Further details on the CO₂ measurement procedure in the ice cores can be found in the studies by Shin (2014) and Lee et al. (2022).

The CH₄ concentrations in the EM blue ice (EM-B, EM-C, and EM-K) were also measured at SNU using the methods of
140 Yang (2019). Following the same pretreatment process as that used for the CO₂ measurements, 45–56 g of ice was placed in a custom-made glass flask. The flask was evacuated for an hour before immersion in hot water to release the trapped air. To prevent CH₄ dissolution, the melted water was refrozen by immersing it in a –80 °C ethanol bath. Finally, the extracted air was analyzed using FID-GC to measure the CH₄ concentrations.

The concentrations of CO₂, CH₄, and N₂O in several ice core samples were also measured along with gas isotopes (δ¹⁵N-N₂,
145 δ¹⁸O-O₂, δO₂/N₂, and δAr/N₂) at the NIPR using wet extraction method. After gas extraction, the gas was split into two aliquots: one for isotope analysis and the other for GHG concentration measurement. CO₂ and CH₄ concentrations were measured using FID-GC, while N₂O concentration was determined with an electron capture detector (ECD) GC. More details can be found in Oyabu et al. (2020) and Lee et al. (2022).

2.6 Stable water isotopes

150 Stable water isotopes (δ¹⁸O_{ice} and δ²H_{ice}) of the surface RM blue ice (approximately 5–10 cm depth) and EM-K core were measured at the Korea Polar Research Institute (KOPRI) using cavity ring-down spectroscopy (CRDS, Picarro L2130-i) (Fig. 1). Ice samples were melted at room temperature and injected into 2 mL vials using disposable syringes equipped with 0.45 μm filters. Measurement precision was achieved by repeatedly measuring the working standard, resulting in a 1σ (standard deviation) of 0.07 ‰ for δ¹⁸O_{ice} and 0.60 ‰ for δ²H_{ice}. Water isotope values were calibrated using the international standards
155 of VSMOW2, SLAP2 (Standard Light Antarctic Precipitation 2), and GISP (Greenland Ice Sheet Precipitation). More details are described in Lee et al. (2022).



3 Results

3.1 Bedrock elevation and ice thickness

The IPR survey revealed a detailed profile of bedrock topography and ice thickness in the EM region and partially in the RM region (Fig. 2). The maximum bedrock elevation reached approximately 1,600 m above mean sea level (AMSL) in both regions, forming a steep and narrow valley between the icefields (Fig. 2a). The ice thickness ranged from 200 m to 800 m within the icefields and from 1,000 to 1,900 m in the valleys (Fig. 2b). Notably, a local bedrock high, approximately 1,000 m AMSL was identified between the Elephant Moraine Main Icefield and the RM regions. This topographic feature may act as a barrier, potentially contributing to differences in the provenance of blue ice between the EM and RM regions.

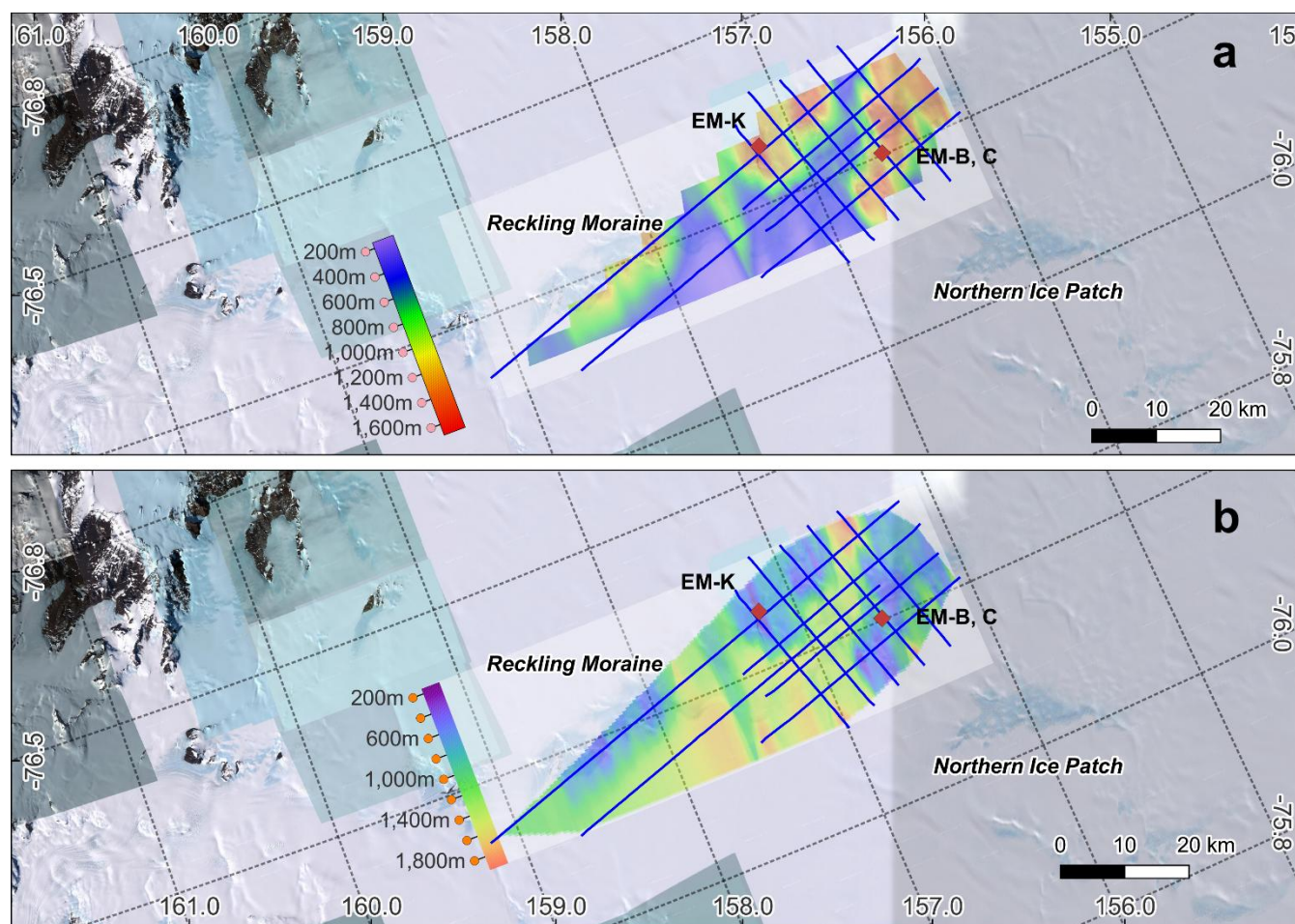


Figure 2. (a) Bedrock elevation and (b) ice thickness of Elephant and Reckling Moraine regions. The blue lines are the survey line of IPR. Red diamonds are the locations of the shallow ice cores drilled. The map was made using a satellite image from © Google Earth in QGIS.



3.2 ^{81}Kr dating

The measured ^{85}Kr activity, a proxy for modern air contamination in the EM-B and EM-C cores was below the detection limit (90 % confidence level), indicating that correction for modern air contamination was not necessary. The resulting ^{81}Kr ages were 101^{+17}_{-17} kyr BP and 108^{+15}_{-14} kyr BP for the analyzed samples of EM-B and EM-C cores, respectively (Table 2). Different from the EM-B and EM-C samples, the air extracted from the EM-K core exhibited ^{85}Kr activity of 5.2 ± 0.4 (dpm cm^{-3}), indicating slight contamination by modern air (Table 2). After modern air correction, assuming that modern air from Seoul was the contamination source, the ^{81}Kr age of the analyzed samples of EM-K core was 351^{+29}_{-26} kyr BP (Table 2). It is important to note that ^{81}Kr ages were given with statistic uncertainties (1σ confidence level) because of atom counting. Additionally, a systematic error arises from the half-life of ^{81}Kr (229 ± 11 kyr) and variations in the past atmospheric ^{81}Kr abundance (Zappala et al., 2020). Considering these uncertainties, the age ranges of analyzed samples of EM-B and EM-C cores were 83–119 kyr BP and 93–124 kyr BP, respectively. The age range of analyzed samples of the EM-K core was 320–385 kyr BP. Since the ^{81}Kr dating was conducted in 2020, its reference point is 2020. This results in a 0.07 kyr difference from the kyr BP notation, which uses 1950 as the reference year. However, this difference was considered negligible in this study.

3.3 $\delta^{15}\text{N-N}_2$, $\delta^{18}\text{O}_{\text{atm}}$, $\delta\text{O}_2/\text{N}_2$, and $\delta\text{Ar}/\text{N}_2$

Ice cores from the Meteorite City Icefield (EM-B and EM-C) and the Elephant Moraine Main Icefield (EM-K) showed distinct values for $\delta^{15}\text{N-N}_2$, $\delta^{18}\text{O}_{\text{atm}}$, $\delta\text{O}_2/\text{N}_2$, and $\delta\text{Ar}/\text{N}_2$ (Table 3). The $\delta^{15}\text{N-N}_2$ values in the EM-B and EM-C cores were lower compared to those in the EM-K core, which may be attributed to a thinner diffusive zone in the firn at the original deposition site of the Meteorite City Icefield compared to that of the Elephant Moraine Main Icefield. The $\delta^{18}\text{O}_{\text{atm}}$ values in the EM-K core were also lower than those in the EM-B and EM-C cores and included a negative value of -0.105 ‰ (Table 3), which indicates a relatively warm period.

The gravity-corrected $\delta\text{O}_2/\text{N}_2$ and $\delta\text{Ar}/\text{N}_2$ values in the EM-B and EM-C cores exhibited significantly high positive values, similar to blue ice samples from Allan Hills in the upper 15 m of ice cores (Spaulding et al., 2013). However, those in the EM-K core were negative, and slightly less positive (Table 3).

Table 3. GHG concentrations and gas isotope ratios of shallow ice from the Elephant Moraine region measured from NIPR using wet extraction method. Only isotopic values were corrected for gravitational fractionation. NA, not available.

Sample	Depth (cm)	TAC (cm^3 STP g^{-1})	CH_4 (ppb)	CO_2 (ppm)	N_2O (ppb)	$\delta^{15}\text{N-N}_2$ (‰)	$\delta^{18}\text{O}_{\text{atm}}$ (‰)	$\delta\text{O}_2/\text{N}_2$ (‰)	$\delta\text{Ar}/\text{N}_2$ (‰)
EM-B	659.0–669.0	0.053	518.9	272.8	257.7	0.248	0.554	10.312	10.434
EM-B	827.5–837.5	NA	NA	NA	NA	0.222	0.495	32.326	24.734
EM-C	416.5–426.5	0.041	521.3	292.9	286.9	0.219	0.399	49.857	34.521
EM-C	558.0–568.0	0.055	518.7	277.0	272.3	0.237	0.503	15.978	11.626



EM-K	247.5–257.5	0.063	485.3	312.0	294.0	0.326	0.286	-1.082	0.229
EM-K	489.5–494.5	0.080	676.9	309.4	297.5	0.378	-0.105	2.717	-1.469

3.4 Greenhouse gases (CO₂, CH₄)

195 The measured CO₂ concentrations in the EM-B and EM-C cores increased toward the surface, exceeding 300 ppm, which is beyond the natural concentration range during the past 800 kyr (180–300 ppm) (Fig. 3, Table S1) (Bereiter et al., 2015). Additionally, CO₂ concentrations higher than 300 ppm were identified at depths of 8.8 m in EM-B and 2.8 m in EM-C, respectively (Fig. 3, Table S1). In the EM-K core, a notably high CO₂ concentration of 628 ppm at a depth of approximately 0.6 m, which is even greater than modern atmospheric CO₂ concentrations, and approximately 350 ppm at 4.7 m depth were identified (Fig. 3, Table S1).

200 The CH₄ concentrations in EM-B and EM-C cores increased toward the surface, exceeding 800 ppb, which is beyond the natural concentration range during the past 800 kyr (340–800 ppb) (Fig. 3, Table S2) (Loulergue et al., 2008). However, at depths greater than 1 m, the measured CH₄ concentrations were in alignment with the natural concentration range during the past 800 kyr (Fig. 3, Table S2). In contrast, the CH₄ concentrations in the EM-K core showed a decreasing trend toward the surface, reaching a very depleted concentration of 207 ppb, which is lower than the natural concentration range during the past 800 kyr. At a depth of 5 m, the EM-K core exhibited a CH₄ concentration of approximately 950 ppb, which is greater than the natural concentration range during the past 800 kyr (Fig. 3, Table S2).

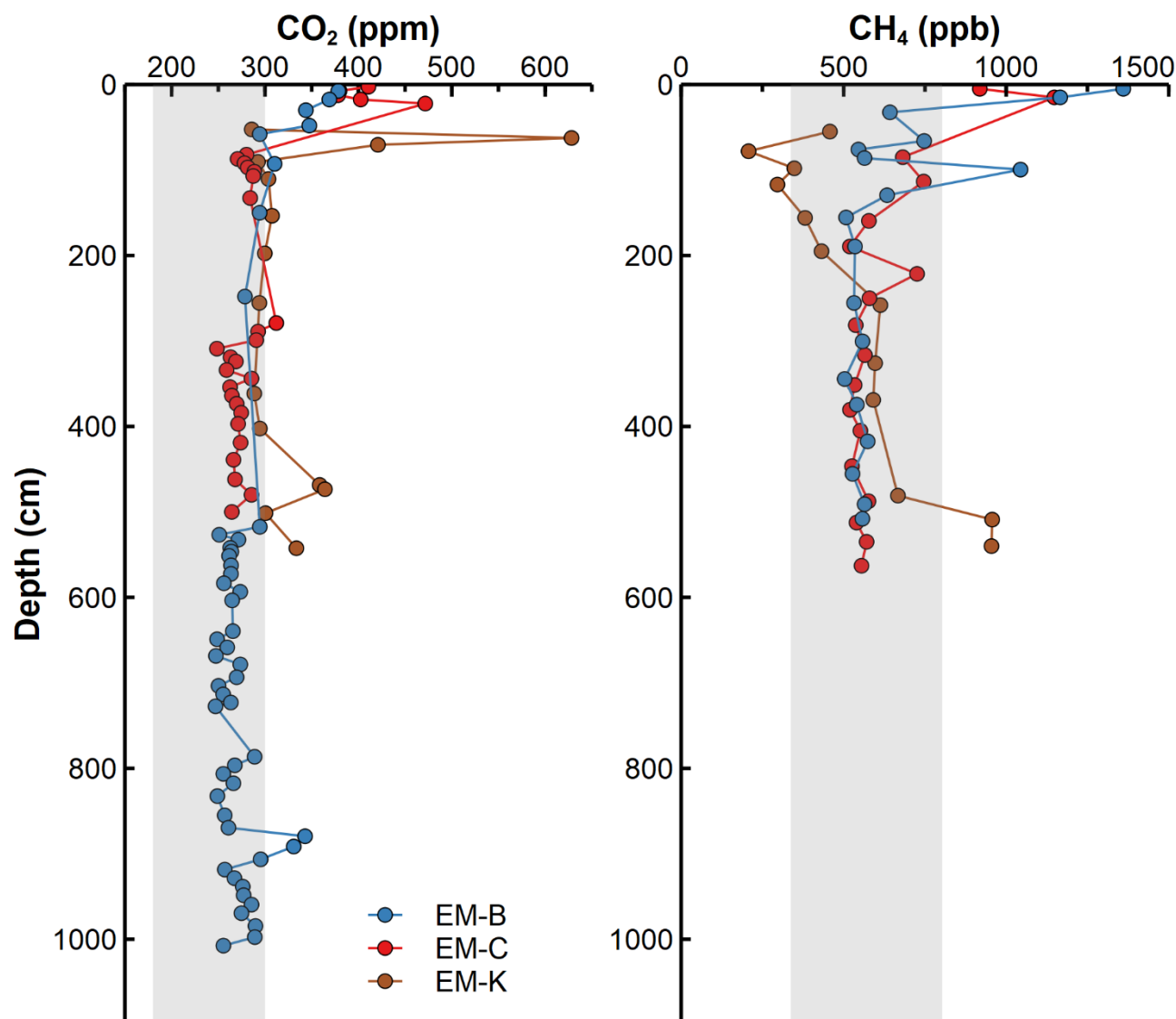


Figure 3. Vertical profiles of CO₂ and CH₄ concentrations in Elephant Moraine blue ice. The CO₂ concentration was measured by a dry-extraction system in SNU. The CH₄ concentration was measured by a wet-extraction system in SNU. The gray shaded area indicates natural concentration range of atmospheric CO₂ and CH₄ during the past 800 kyr.

3.5 Stable water isotopes

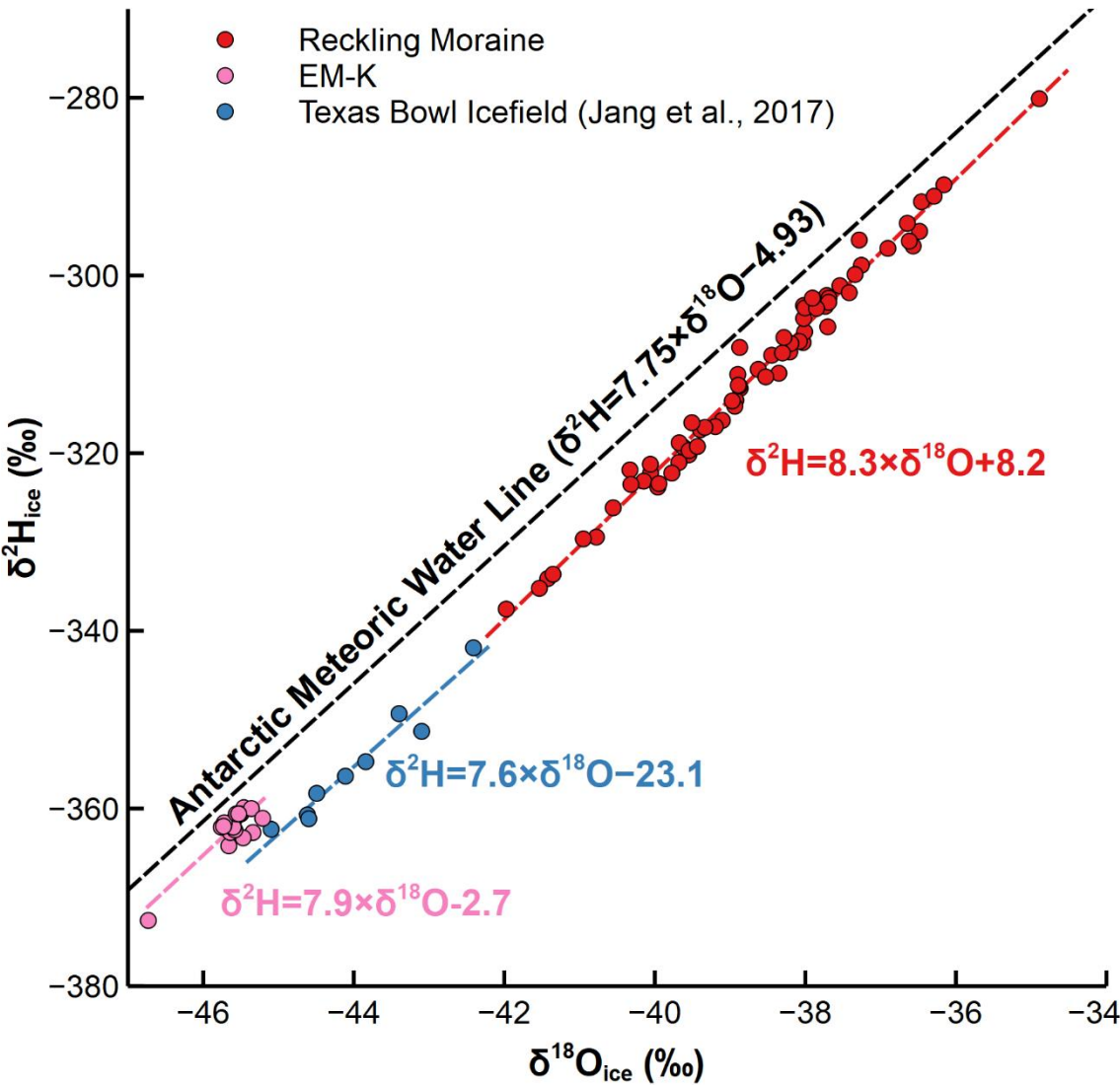
The stable water isotope measurements ($\delta^{18}\text{O}_{\text{ice}}$ and $\delta^2\text{H}_{\text{ice}}$) of RM blue ice showed no discernible increasing or decreasing trend along the transect (Fig. S1). The average $\delta^{18}\text{O}_{\text{ice}}$ and $\delta^2\text{H}_{\text{ice}}$ values of RM blue ice were $-38.6 \pm 1.4 \text{ ‰}$ (1σ) and $-311.0 \pm 11.8 \text{ ‰}$ (1σ), respectively (Table S3). The average $\delta^{18}\text{O}_{\text{ice}}$ and $\delta^2\text{H}_{\text{ice}}$ values of EM-K blue ice were $-45.6 \pm 0.3 \text{ ‰}$ (1σ) and $-362.2 \pm 2.6 \text{ ‰}$ (1σ), respectively (Table S4).



Compared to $\delta^{18}\text{O}_{\text{ice}}$ measurements from ice sampled around Reckling Peak, which ranged from -51.2‰ to -41.2‰ (Faure et al., 1992), our measured RM blue ice $\delta^{18}\text{O}_{\text{ice}}$ values were relatively higher, ranging from -42.0‰ to -34.9‰ . Since the typical glacial-interglacial $\delta^{18}\text{O}_{\text{ice}}$ difference in East Antarctica is $5\text{--}6\text{‰}$ (Stenni et al., 2010), the very wide $\delta^{18}\text{O}_{\text{ice}}$ range observed in RM blue ice (from -51.2‰ to -34.9‰) suggested significant differences in provenance of blue ice.

220 The EM-K core showed the most negative $\delta^{18}\text{O}_{\text{ice}}$ values (Fig. 4), suggesting that surface snow at the original deposition site of the Elephant Moraine Main Icefield experienced colder conditions than those at nearby icefields (Texas Bowl and RM blue ice). In contrast, the RM blue ice had the most enriched water isotope values (Fig. 4), suggesting that its origin experienced warmer conditions than those of the Elephant Moraine Main Icefield and Texas Bowl blue ice.

The deuterium excess ($d\text{-excess} = \delta^2\text{H}_{\text{ice}} - 8 \times \delta^{18}\text{O}_{\text{ice}}$) values exhibited negative values in both the RM and Texas Bowl
225 blue ice samples (Table S3) (Jang et al., 2017). RM blue ice showed an average of $-1.8 \pm 1.5\text{‰}$ (1σ) (Table S3), while Texas Bowl blue ice exhibited even more negative $d\text{-excess}$ values, averaging $-3.4 \pm 1.4\text{‰}$ (1σ) (Fig. 4) (Jang et al., 2017). The $d\text{-excess}$ can be influenced by the source of the water vapor, supersaturation during cloud formation, and post-depositional alterations such as sublimation. Recent finding indicated that sublimation significantly contributed to negative $d\text{-excess}$ values observed in surface snow and ice near the Dry Valleys in Antarctica (Hu et al., 2022). Therefore, it is plausible that isotope
230 fractionation driven by sublimation also impacted the original deposition sites of RM and Texas Bowl blue ice samples. The EM-K core on the other hand, showed a positive $d\text{-excess}$ value of $2.7 \pm 1.3\text{‰}$ (1σ), suggesting relatively less isotope fractionation because of sublimation at the original deposition site of Elephant Moraine Main Icefield than those of RM and Texas Bowl Icefields.



235 **Figure 4.** Stable water isotope bi-plot comparing the RM blue ice measurements and Elephant Moraine blue ice with the Antarctic Meteoric Water Line (Masson-Delmotte et al., 2008).

4 Discussions

4.1 Altered gas records in surface EM blue ice

4.1.1 Relatively low total air content (TAC)

240 The TAC of EM blue ice was derived as a by-product of air sampling for ^{81}Kr dating at USTC and GHG measurements at NIPR, with values ranging from 0.041 to 0.080 $\text{cm}^3 \text{g}^{-1}$ (Table 2 and 3). These values are substantially lower than those



observed in deep Antarctic ice cores, which typically range from 0.080 to 0.118 cm³ g⁻¹ (Raynaud and Whillans, 1982; Martinerie et al., 1994; Delmotte et al., 1999; Raynaud et al., 2007). One reason for the low TAC is partial melting. However, no melt layers were visually observed in the EM ice cores, and the maximum austral summer air temperature of -9.5 °C in the EM region suggests that partial melting is unlikely (Fig. S2). Furthermore, the original deposition site of the EM blue ice is likely situated further inland, where colder conditions would have prevented surface snow melting. Despite the absence of visible melt layers, line scanning is warranted to detect any potential small-scale melt layers that could result from sunlight penetration into blue ice (Cooper et al., 2021). Further studies should also investigate the possibility for gas loss during storage, as the ice cores were kept at temperatures above -50 °C (Oyabu et al., 2021). Gas loss may have also occurred when the ice was exposed at the surface, considering the annual mean temperature of the area is -30.3 °C (Lee et al., 2022).

4.1.2 Significantly high positive $\delta\text{O}_2/\text{N}_2$ and $\delta\text{Ar}/\text{N}_2$ values

Typical bubbly ice samples from deep ice cores exhibit negative $\delta\text{O}_2/\text{N}_2$ and $\delta\text{Ar}/\text{N}_2$ values, ranging from -15 ‰ to 0 ‰ (Landais et al., 2012; Extier et al., 2018; Oyabu et al., 2021). In bubbly ice samples, these values can become even more depleted if gas loss occurs during storage (Oyabu et al., 2021). In this context, the positive $\delta\text{O}_2/\text{N}_2$ and $\delta\text{Ar}/\text{N}_2$ values observed in bubbly blue ice samples from EM (Table 3) and Allan Hills BIA are unusual (Spaulding et al., 2013). To explain the positive values observed in the bubbly blue ice samples, Spaulding et al. (2013) suggested two possibilities: (1) the preferential loss of N₂ or (2) the addition of O₂ and Ar. However, the idea of preferential N₂ loss is questionable because O₂ and Ar have higher diffusion coefficient than N₂ in ice (Ikeda-Fukazawa et al., 2004). The addition of O₂ and Ar could have occurred because of surface snow melting at the original deposition site, given that O₂ and Ar are more soluble than N₂ (Hamme and Emerson, 2004). If then, the measured $\delta^{18}\text{O}_{\text{atm}}$ value would also be affected. However, it is difficult to determine whether it is depleted or enriched relative to its original value. If the snowmelt refroze after reaching equilibrium with atmospheric air, ¹⁸O would have preferentially dissolved over ¹⁶O, whereas if it refroze before reaching equilibrium, ¹⁶O would have dissolved preferentially over ¹⁸O (Li et al., 2019). However, as discussed in Sect. 4.1.1, surface snow melting at the original deposition site is considered unlikely. Further investigation is needed to understand the positive $\delta\text{O}_2/\text{N}_2$ and $\delta\text{Ar}/\text{N}_2$ values observed in blue ice samples.

4.1.3 Enriched and depleted GHG concentrations

The enriched GHG concentrations at shallow depths (<1 m) in the EM-B and EM-C cores may be associated with the presence of a visible dust band, observed at depths of 0–20 cm in EM-B and 76 cm in EM-C (Jang et al., 2017). A study using blue ice in Pakitsoq, western Greenland also revealed that enriched CH₄ values were correlated with visible dust bands, but the mechanism remained unclear (Petrenko et al., 2006). The elevated GHG concentrations around a depth of 5 m in the EM-K core are attributed to modern air intrusion, as indicated by the ⁸⁵Kr activity value (Table 2). If the positive $\delta\text{O}_2/\text{N}_2$ and $\delta\text{Ar}/\text{N}_2$ values in EM blue ice result from surface snow melting, the enriched GHG concentrations may also be associated with this process, as CO₂ and CH₄ are more soluble than the major components of air (Wilhelm et al., 1977). Further investigation is



required to better understand the cause of GHG alterations in EM blue ice, particularly the very high CO₂ concentration (628
275 ppm) and unusually low CH₄ concentration (207 ppb) in the EM-K core.

4.2 Age constraints of Elephant Moraine blue ice

Based on ⁸¹Kr dating, the shallow ice cores from the Meteorite City Icefield (EM-B and EM-C) correspond to Marine Isotope
Stage (MIS) 5, while the shallow ice core from the Elephant Moraine Main Icefield (EM-K) corresponds to MIS 9–11 (Fig.
5). Although the GHG concentrations and $\delta^{18}\text{O}_{\text{atm}}$ values of the EM blue ice are not pristine, we compared them with unaltered
280 records from Antarctic deep ice cores to further constrain the age of the EM blue ice (Fig. 5). For this comparison, we used
the measurement results from depths greater than 3 m, excluding those that fall outside the natural range during the past 800
kyr. However, based on the scattered distribution of GHG concentrations, even at depths greater than 3 m (Fig. 3), the
measurement results may still be altered from their original values. Nevertheless, based on the average and standard deviation
of these values, EM-B and EM-C cores do not correspond strongly to MIS 5e (Fig. 5). Similarly, the ice from EM-K core is
285 unlikely to correspond to the period of MIS 10–11 and may instead be from MIS 9 (Fig. 5).

The Elephant Moraine Main Icefield contains older surface ice than the Allan Hills BIA, where the surface ice age ranges
90–250 kyr BP (Spaulding et al., 2013). Considering that an ice age of 6 Myr BP has been identified at a depth of 200 m in
the Allan Hills BIA (Higgins et al., 2025), the Elephant Moraine Main Icefield presents a strong potential for preserving ancient
ice from the MPT period at ice depths of a few hundred meters.

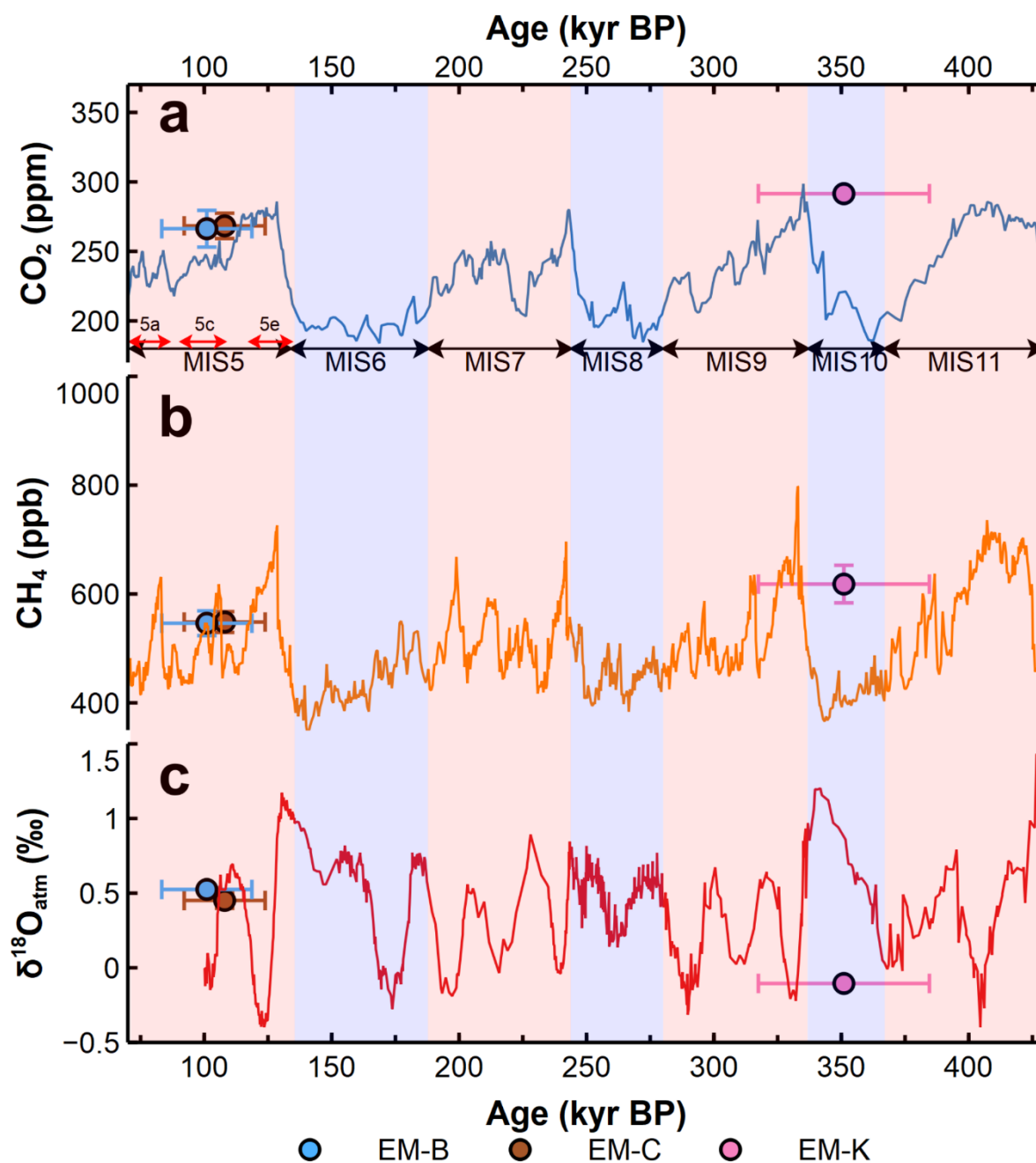


Figure 5. Gas composition comparison between EM blue ice and published records from Antarctic ice cores. Horizontal bars for age are the full range of ⁸¹Kr age of analyzed samples of EM-B, EM-C, and EM-K core, considering systematic error together (Table 2). Error bars for CO₂, CH₄, and δ¹⁸O_{atm} represent 1σ standard deviation. **(a)** Blue line is the CO₂ composite data from Bereiter et al. (2015). The Marine isotope stage (MIS) numbers are written at the bottom of the panel (Raisbeck et al., 2015). **(b)** Orange line is the CH₄ concentrations measured from the EDC core (Loulergue et al., 2008). **(c)** Red line is the δ¹⁸O_{atm} measured from the EDC core (Extier et al., 2018).



5 Conclusions

In this study, we investigated the blue ice in the Elephant Moraine and Reckling Moraine regions of East Antarctica. The IPR survey revealed that the bedrock elevations reached approximately 1,600 m, while the ice thickness ranged from 200 m to 800 m across the icefields. The ^{81}Kr dating results indicated ages of 83–119 kyr BP and 93–124 kyr BP for blue ice in the Meteorite City Icefield and 320–385 kyr BP for blue ice in the Elephant Moraine Main Icefield. The comparison of stable water isotopes indicated that the original deposition site of the Elephant Moraine Main Icefield experienced colder condition than those of the Texas Bowl and Reckling Moraine Icefield. Stable water isotope measurements of blue ice in the Reckling Moraine region showed negative deuterium excess values, indicating that the surface snow at its original deposition site experienced isotope fractionation. The blue ice in the Elephant Moraine region exhibited a very low TAC along with positive $\delta\text{O}_2/\text{N}_2$ and $\delta\text{Ar}/\text{N}_2$ values, the causes of which are not yet clearly understood. Additionally, the measured GHG concentrations showed significant alterations, possibly related to high dust content and modern air contamination. Further age constraints, based on comparisons of CO_2 , CH_4 , and $\delta^{18}\text{O}_{\text{atm}}$ measurements with those from Antarctic deep ice cores, suggested that the surface blue ice in the Elephant Moraine Main Icefield may correspond to MIS 9. Although pristine gas records are required for more accurate age constraints, we suggest that the Elephant Moraine Main Icefield is a highly promising area for discovering ancient ice spanning the Mid-Pleistocene Transition period.

Data availability

All data are presented in the main text and in the supplement.

Author contribution

GL conceived the idea of this study, measured greenhouse gas concentrations, and wrote the manuscript with contributions from all co-authors. JA conceived the idea of this study and interpreted the data. HJ, JL and SDH conducted the ice-penetrating radar survey and data processing. IO and KK measured isotopes of gas components. FR, ZTL, WJ, and GMY performed the ^{81}Kr age dating. SK, JM, and YH measured the stable water isotopes.

Competing interests

The authors declare that they have no conflict of interest.



320 Acknowledgments

This study is based on Giyeon Lee's (first author) 2024 doctoral dissertation at Seoul National University. We thank Sang-Young Han, Yoojung Yang, Youngjoon Jang, and Yeongjun Ryu for ice collection in the Elephant Moraine and Reckling Moraine region. We also thank Nayeon Ko, Jinhwa Shin, Junghwa Hwang, and Kwangjin Yim for their laboratory assistance and technical support. We acknowledge the Norwegian Polar Institute's Quantarctica package. Lastly, we would like to thank
325 Editage (www.editage.co.kr) for English language editing.

Financial support

This study received financial support from the National Research Foundation of Korea (NRF) (grant no. RS-2024-00449415; RS-2023-00278926; RS-2023-00291696). The Ministry of Science and Technology of China (MOST), Innovation Program for Quantum Science and Technology (2021ZD0303101), the National Natural Science Foundation of China (T2325024,
330 41727901). This work was also supported by Korea Polar Research Institute (KOPRI) grant funded by the Ministry of Oceans and Fisheries (KOPRI PE25100).

References

- Ahn, J., Brook, E. J., and Howell, K.: A high-precision method for measurement of paleoatmospheric CO₂ in small polar ice samples, *J. Glaciol.*, 55, 499–506, <https://doi.org/10.3189/002214309788816731>, 2009.
- 335 Bender, M., Sowers, T. and Lipenkov, V.: On the concentrations of O₂, N₂, and Ar in trapped gases from ice cores, *J. Geophys. Res.-Atmos.*, 100, 18651–18660, <https://doi.org/10.1029/94JD02212>, 1995.
- Bereiter, B., Eggelston, S., Schmitt, J., Nehrbass-Ahles, C., Stocker, T. F., Fischer, H., Kipfstuhl, S., and Chappellaz, J.: Revision of the EPICA Dome C CO₂ record from 800 to 600 kyr before present, *Geophys. Res. Lett.*, 42, 542–549, <https://doi.org/10.1002/2014GL061957>, 2015.
- 340 Buizert, C., Baggenstos, D., Jiang, W., Purtschert, R., Petrenko, V. V., Lu, Z.-T., Müller, P., Kuhl, T., Lee, J., Severinghaus, J. P., and Brook, E. J.: Radiometric ⁸¹Kr dating identifies 120,000-year-old ice at Taylor Glacier, Antarctica, *P. Natl. Acad. Sci. USA.*, 111, 6876–6881, <https://doi.org/10.1073/pnas.1320329111>, 2014.
- Capron, E., Landais, A., Leieux-Dudon, B., Schilt, A., Masson-Delmotte, V., Buiron, D., Chappellaz, J., Dahl-Jensen, D., Johnsen, S., Leuenberger, M., Loulergue, L., and Oerter, H.: Synchronising EDML and NorthGRIP ice cores using δ¹⁸O
345 of atmospheric oxygen (δ¹⁸O_{atm}) and CH₄ measurements over MIS5 (80–123 kyr), *Quaternary Sci. Rev.*, 29, 222–234, <https://doi.org/10.1016/j.quascirev.2009.07.014>, 2010.
- Cassidy, W., Harvey, R., Schutt, J., Delisle, G., and Yanai, K.: The meteorite collection sites of Antarctica, *Meteoritics*, 27, 490–525, <https://doi.org/10.1111/j.1945-5100.1992.tb01073.x>, 1992.



- Cooper, M. G., Smith, L. C., Rennermalm, A. K., Tedesco, M., Muthyala, R., Leidman, S. Z., Moustafa, S. E., and Fayne, J.
350 V.: Spectral attenuation coefficients from measurements of light transmission in bare ice on the Greenland Ice Sheet,
Cryosphere, 15, 1931–1953, <https://doi.org/10.5194/tc-15-1931-2021>, 2021.
- Craig, H., Horibe, Y., and Sowers, T.: Gravitational separation of gases and isotopes in polar ice caps, *Science*, 242, 1675–
1678, <https://doi.org/10.1126/science.242.4886.1675>, 1988.
- Delmotte, M., Raynaud, D., Morgan, V., and Jouzel, J.: Climatic and glaciological information inferred from air-content
355 measurements of a Law Dome (East Antarctica) ice core, *J. Glaciol.*, 45, 255–263,
<https://doi.org/10.3189/002214399793377031>, 1999.
- Dunbar, N. W., McIntosh, W. C., and Esser, R. P.: Physical setting and tephrochronology of the summit caldera ice record at
Mount Moulton, West Antarctica, *Geol. Soc. Am. Bull.*, 120, 796–812, <https://doi.org/10.1130/B26140.1>, 2008.
- EPICA community members: Eight glacial cycles from an Antarctic ice core, *Nature*, 429, 623–628,
360 <https://doi.org/10.1038/nature02599>, 2004.
- Extier, T. Landais, A., Bréant, C., Prié, F., Bazin, L., Dreyfus, G., Roche, D. M., Leuenberger, B.: On the use of $\delta^{18}\text{O}_{\text{atm}}$ for
ice core dating, *Quaternary Sci. Rev.*, 185, 244–257, <https://doi.org/10.1016/j.quascirev.2018.02.008>, 2018.
- Faure, G. and Buchanan, D.: Ablation rates of the ice fields in the vicinity of the Allan Hills, Victoria Land, Antarctica,
Contributions to Antarctic Research II, 53, 19–31, <https://doi.org/10.1029/AR053p0019>, 1991.
- 365 Faure, G., Grootes, P., Buchanan, D., and Hagen, E. H.: Oxygen isotope study of the ice fields surrounding the Reckling
Moraine on the East Antarctic ice sheet, *Contributions to Antarctic Research III*, 57, 15–26,
<https://doi.org/10.1029/AR057p0015>, 1992.
- Fischer, H., Severinghaus, J., Brook, E., Wolff, E., Albert, M., Alemany, O., Arthern, R., Bentley, C., Blankenship, D.,
Chappellaz, J., Creyts, T., Dahl-Jensen, D., Dinn, M., Frezzotti, M., Fujita, S., Galée, H., Hindmarsh, R., Hudspeth, D.,
370 Jugie, G., Kawamura, K., Lipenkov, V., Miller, H., Mulvaney, R., Parrenin, F., Pattyn, F., Ritz, C., Schwander, J.,
Steinhage, D., van Ommen, T., and Wilhelms, F.: Where to find 1.5 million yr old ice for the IPICS “Oldest-Ice” ice core,
Clim. Past, 9, 2489–2505, <https://doi.org/10.5194/cp-9-2489-2013>, 2013.
- Folco, L., Welten, K. C., Jull, A. J. T., Nishiizumi, K., and Zeoli, A.: Meteorites constrain the age of Antarctic ice at the
Frontier Mountain blue ice field (northern Victoria Land), *Earth Planet Sc. Lett.*, 248, 209–216,
375 <https://doi.org/10.1016/j.epsl.2006.05.022>, 2006.
- Gardner, A. S., Moholdt, G., Scambos, T., Fahnestock, M., Ligtenberg, S., van den Broeke, M., and Nilsson, J.: Increased West
Antarctic and unchanged East Antarctic ice discharge over the last 7 years, *Cryosphere*, 12, 521–547,
<https://doi.org/10.5194/tc-12-521-2018>, 2018.
- Goujon, C., Barnola, J.-M., and Ritz, C.: Modeling the densification of polar firn including heat diffusion: Application to close-
380 off characteristics and gas isotopic fractionation for Antarctica and Greenland sites, *J. Geophys. Res.-Atmos.*, 108, 4792,
<https://doi.org/10.1029/2002JD003319>, 2003.



- Hamme, R. C., and Emerson, S. R.: The solubility of neon, nitrogen and argon in distilled water and seawater, Deep Sea Research Part I: Oceanographic Research Papers, 51, 1517–1528, <https://doi.org/10.1016/j.dsr.2004.06.009>, 2004.
- Higgins, J., Shackleton, S., Hishamunda, V., Davidge, L., Brook, E., Peterson, J. M., Carter, A., Aarons, S., Kurbatov, A. V.,
385 Introne, D., Yan, Y., Buizert, C., Steig, E., Schauer, A., Morgan, J., Severinghaus, J., Bender, M., Neff, P., and Epifanio, J.: Miocene and Pliocene ice and air from the Allan Hills blue ice area, East Antarctica, ESS Open Archive [preprint], <https://doi.org/10.22541/essoar.173897232.24923969/v1>, 07 February 2025.
- Hu, J., Yan, Y., Yeung, L. Y., and Dee, S. G.: Sublimation origin of negative deuterium excess observed in snow and ice samples from McMurdo Dry Valleys and Allan Hills blue ice areas, East Antarctica, J. Geophys. Res.-Atmos., 127,
390 e2021JD035950, <https://doi.org/10.1029/2021JD035950>, 2022.
- Hu, Z., Jiang, W., Yan, Y., Huang, Y., Tang, X., Li, L., Ritterbusch, F., Yang, G.-M., Lu, Z.-T., and Shi, G.: Brief communication: Identification of 140000-year-old blue ice in the Grove Mountains, East Antarctica, by krypton-81 dating, Cryosphere, 18, 1647–1652, <https://doi.org/10.5194/tc-18-1647-2024>, 2024.
- Hui, F., Ci, T., Cheng, X., Scambo, T. A., Liu, Y., Zhang, Y., Chi, Z., Huang H., Wang, X., Wang, F., Zhao, C., Jin, Z., and
395 Wang, K.: Mapping blue-ice areas in Antarctica using ETM+ and MODIS data, Ann. Glaciol., 55, 129–137, <https://doi.org/10.3189/2014AoG66A069>, 2014.
- Ikeda-Fukazawa, T., Hondoh, T., Fukumura, T., Fukazawa, H., and Mae, S.: Variation in N₂/O₂ ratio of occluded air in Dome Fuji antarctic ice, J. Geophys. Res.-Atmos., 106, 17799–17810, <https://doi.org/10.1029/2000JD000104>, 2001.
- Ikeda-Fukazawa, T., Kawamura, K., and Hondoh, T.: Mechanism of molecular diffusion in ice crystals, Mol. Simulat., 30,
400 973–979, <https://doi.org/10.1080/08927020410001709307>, 2004.
- Ikeda-Fukazawa, T., Fukumizu, K., Kawamura, K., Aoki, S., Nakazawa, T., and Hondoh, T.: Effects of molecular diffusion on trapped gas composition in polar ice cores, Earth Planet. Sc. Lett., 299, 183–192, <https://doi.org/10.1016/j.epsl.2004.11.011>, 2005.
- Jang, Y., Ryu, Y., Yang, J.-W., Lee, H.-G., and Ahn, J.: A preliminary study for blue ice in Victoria Land, East Antarctica, Journal of the Geological Society of Korea, 53, 567–580, <https://doi.org/10.14770/jgsk.2017.53.4.567>, 2017.
- Jiang, W., Bailey, K., Lu, Z.-T., Mueller, P., O'Connor, T. P., Cheng, C.-F., Hu, S.-M., Purtschert, R., Sturchio, N. C., Sun, Y. R., Williams, W. D., Yang, G.-M.: An atom counter for measuring ⁸¹Kr and ⁸⁵Kr in environmental samples, Geochim. Cosmochim. Ac., 91, 1–6, <https://doi.org/10.1016/j.gca.2012.05.019>, 2012.
- Korotkikh, E. V., Mayewski, P. A., Handley, M. J., Sneed, S. B., Introne, D. S., Kurbatov, A. V., Dunbar, N. W., and McIntosh, W. C.: The last interglacial as represented in the glaciochemical record from Mount Moulton Blue Ice Area, West
410 Antarctica, Quaternary Sci. Rev., 30, 1940–1947, <https://doi.org/10.1016/j.quascirev.2011.04.020>, 2011.
- Landais, A., Caillon, N., Severinghaus, J., Jouzel, J., and Masson-Delmotte, V.: Analyses isotopiques à haute précision de l'air piégé dans les glaces polaires pour la quantification des variations rapides de température: méthodes et limites, Notes



- des activités instrumentales de l'IPSL, 39, <https://hal.archives-ouvertes.fr/hal-03263858/document> (last access: 21 January
415 2025), 2003.
- Landais, A., Dreyfus, G., Capron, E., Pol, K., Loutre, M. F., Raynaud, D., Lipenkov, V. Y., Arnaud, L., Masson-Delmotte, V.,
Paillard, D., Jouzel, J., and Leuenberger, M.: Towards orbital dating of the EPICA Dome C ice core using $\delta\text{O}_2/\text{N}_2$, *Clim.*
Past, 8, 191–203, <https://doi.org/10.5194/cp-8-191-2012>, 2012.
- Lee, G., Ahn, J., Ju, H., Ritterbusch, F., Oyabu, I., Buizert, C., Kim, S., Moon, J., Ghosh, S., Kawamura, K., Lu, Z.-T., Hong,
420 S., Han, C. H., Hur, S. D., Jiang, W., and Yang, G.-M.: Chronostratigraphy of the Larsen blue-ice area in northern Victoria
Land, East Antarctica, and its implications for paleoclimate, *Cryosphere*, 16, 2301–2324, <https://doi.org/10.5194/tc-16-2301-2022>, 2022.
- Lee, J. E., Edwards, J. S., Schmitt, J., Fischer, H., Bock, M., and Brook, E. J.: Excess methane in Greenland ice cores associated
with high dust concentrations, *Geochim. Cosmochim. Ac.*, 270, 409–430, <https://doi.org/10.1016/j.gca.2019.11.020>, 2020.
- 425 Li, B., Yeung, L. Y., Hu, H., and Ash, J. L.: Kinetic and equilibrium fractionation of O_2 isotopologues during air-water gas
transfer and implications for tracing oxygen cycling in the ocean, *Mar. Chem.*, 210, 61–71,
<https://doi.org/10.1016/j.marchem.2019.02.006>, 2019.
- Lilien, D. A., Steinhage, D., Taylor, D., Parrenin, F., Ritz, C., Mulvaney, R., Martin, C., Yan, J.-B., O'Neill, C., Frezzotti, M.,
Miller, H., Gogineni, P., Dahl-Jensen, D., and Eisen, O.: Brief communication: New radar constraints support presence of
430 ice older than 1.5 Myr at Little Dome C, *Cryosphere*, 15, 1881–1888, <https://doi.org/10.5194/tc-15-1881-2021>, 2021.
- Martinerie, P., Lipenkov, V. Y., Raynaud, D., Chappellaz, J., Barkov, N. I., and Lorius, C.: Air content paleo record in the
Vostok ice core (Antarctica): A mixed record of climatic and glaciological parameters, *J. Geophys. Res.-Atmos.*, 99,
10565–10576, <https://doi.org/10.1029/93JD03223>, 1994.
- Masson-Delmotte, V., Hou, S., Ekaykin, A., Jouzel, J., Aristarain, A., Bernardo, R. T., Bromwich, D., Cattani, O., Delmotte,
435 M., Falourd, S., Frezzotti, M., Gallée, H., Genoni, L., Isaksson, E., Landais, A., Helsen, M. M., Hoffmann, G., Lopez, J.,
Morgan, V., Motoyama, H., Noone, D., Oerter, H., Petit, J. R., Royer, A., Uemura, R., Schmidt, G. A., Schlosser, E.,
Simões, J. C., Steig, E. J., Stenni, B., Stievenard, M., van den Broeke, M. R., van de Wal, R. S. W., van de Berg, W. J.,
Vimeux, F., and White, J. W. C.: A review of Antarctic surface snow isotopic composition: observations, atmospheric
circulation, and isotopic modelling, *J. Climate*, 21, 3359–3387, <https://doi.org/10.1175/2007JCLI2139.1>, 2008.
- 440 Moore, J. C., Nishio, F., Fujita, S., Narita, H., Pasteur, E., Grinsted, A., Sinisalo, A., and Maeno, N.: Interpreting ancient ice
in a shallow ice core from the South Yamato (Antarctica) blue ice area using flow modelling and compositional matching
to deep ice cores, *J. Geophys. Res.-Atmos.*, 111, D16302, <https://doi.org/10.1029/2005JD006343>, 2006.
- Mouginot, J., Scheuchl, B., and Rignot, E.: Mapping of ice motion in Antarctica using synthetic-aperture radar data, *Remote
Sensing*, 4, 2753–2767, <https://doi.org/10.3390/rs4092753>, 2012.
- 445 NEEM community members: Eemian interglacial reconstructed from a Greenland folded ice core, *Nature*, 493, 489–494,
<https://doi.org/10.1038/nature11789>, 2013.



- Oyabu, I., Kawamura, K., Kitamura, K., Dallmayr, R., Kitamura, A., Sawada, C., Severinghaus, J. P., Beaudette, R., Orsi, A., Sugawara, S., Ishidoya, S., Dahl-Jensen, D., Goto-Azuma, K., Aoki, S., and Nakazawa, T.: New technique for high-precision, simultaneous measurements of CH₄, N₂O and CO₂ concentrations; isotopic and elemental ratios of N₂, O₂ and Ar; and total air content in ice cores by wet extraction, *Atmos. Meas. Tech.*, 13, 6703–6731, <https://doi.org/10.5194/amt-13-6703-2020>, 2020.
- Oyabu, I., Kawamura, K., Uchida, T., Fujita, S., Kitamura, K., Hirabayashi, M., Aoki, S., Morimoto, S., Nakazawa, T., Severinghaus, J. P., and Morgan, J. D.: Fractionation of O₂/N₂ and Ar/N₂ in the Antarctic ice sheet during bubble formation and bubble–clathrate hydrate transition from precise gas measurements of the Dome Fuji ice core, *Cryosphere*, 15, 5529–5555, <https://doi.org/10.5194/tc-15-5529-2021>, 2021.
- Petrenko, V. V., Severinghaus, J. P., Brook, E. J., Reeh, N., and Schaefer, H.: Gas records from the West Greenland ice margin covering the Last Glacial Termination: a horizontal ice core, *Quaternary Sci. Rev.*, 25, 865–875, <https://doi.org/10.1016/j.quascirev.2005.09.005>, 2006.
- Railsback, L. B., Gibbard, P. L., Head, M. J., Voarintsoa, N. R. G., and Toucanne, S.: An optimized scheme of lettered marine isotope substages for the last 1.0 million years, and the climatostratigraphic nature of isotope stages and substages, *Quaternary Sci. Rev.*, 111, 94–106, <https://doi.org/10.1016/j.quascirev.2015.01.012>, 2015.
- Raynaud, D. and Whillans, I. M.: Air content of the Byrd core and past changes in the West Antarctic Ice Sheet, *Ann. Glaciol.*, 3, 269–273, <https://doi.org/10.3189/S0260305500002901>, 1982.
- Raynaud, D., Lipenkov, V., Lemieux-Dudon, B., Duval, P., Loutre, M.-F., and Lhomme, N.: The local insolation signature of air content in Antarctic ice. A new step toward an absolute dating of ice records, *Earth Planet. Sc. Lett.*, 261, 337–349, <https://doi.org/10.1016/j.epsl.2007.06.025>, 2007.
- Reynolds, J. M.: *An Introduction to Applied and Environmental Geophysics*, 2nd edition, Wiley, 712 pp., ISBN 978-0-470-97544-2, 2011.
- Rignot, E., Mouginot, J., and Scheuchl, B.: Ice flow of the Antarctic ice sheet, *Science*, 333, 1427–1430, <https://doi.org/10.1126/science.1208336>, 2011.
- Righter, K., Schutt, J., Lunning, N., Harvey, R., and Karner, J.: Identification and pairing reassessment of unequilibrated ordinary chondrites from four Antarctic dense collection areas, *Meteorit. Planet. Sci.*, 56, 1556–1573, <https://doi.org/10.1111/maps.13707>, 2021.
- Schwander, J. and Stauffer, B.: Age difference between polar ice and the air trapped in its bubbles, *Nature*, 311, 45–47, <https://doi.org/10.1038/311045a0>, 1984.
- Severinghaus, J. P., Sowers, T., Brook, E. J., Alley, R. B., and Bender, M. L.: Timing of abrupt climate change at the end of the Younger Dryas interval from thermally fractionated gases in polar ice, *Nature*, 391, 141–146, <https://doi.org/10.1038/34346>, 1998.
- Severinghaus, J. P., Beaudette, R., Headly, M. A., Taylor, K., and Brook, E. J.: Oxygen-18 of O₂ records the impact of abrupt climate change on the terrestrial biosphere, *Science*, 324, 1431–1434, <https://doi.org/10.1126/science.1169473>, 2009.



- Shin, J.: Atmospheric CO₂ variations on millennial time scales during the early Holocene, MS thesis, School of Earth and Environmental Sciences, Seoul National University, South Korea, chrome-extension://efaidnbmnnnibpcajpcglclefindmkaj/https://s-space.snu.ac.kr/bitstream/10371/131380/1/000000017635.pdf (last access: 04 February 2025), 2014.
- 485 Shin, J., Ahn, J., Beeman, J. C., Lee, H.-G., Seo, J. M., and Brook, E. J.: Millennial variations in atmospheric CO₂ during the early Holocene (11.7–7.4 ka), *Clim. Past*, 18, 2063–2075, <https://doi.org/10.5194/cp-18-2063-2022>, 2022.
- Sinisalo, A., Grinsted, A., Moore, J., Meijer, H., Martma, T., and Van De Wal, R. S. W.: Inferences from stable water isotopes on the Holocene evolution of Scharffenbergbotnen blue-ice area, East Antarctica, *J. Glaciol.*, 53, 427–434, <https://doi.org/10.3189/002214307783258495>, 2007.
- 490 Sinisalo, A. and Moore, J. C.: Antarctic blue ice areas - towards extracting palaeoclimate information, *Antarct. Sci.*, 22, 99–115, <https://doi.org/10.1017/S0954102009990691>, 2010.
- Spaulding, N. E., Higgins, J. A., Kurbatov, A. V., Bender, M. L., Arcone, S. A., Campbell, S., Dunbar, N. W., Chimiak, L. M., Introne, D. S., and Mayewski, P. A.: Climate archives from 90 to 250 ka in horizontal and vertical ice cores from the Allan Hills Blue Ice Area, Antarctica, *Quaternary Res.*, 80, 562–574, <https://doi.org/10.1016/j.yqres.2013.07.004>, 2013.
- 495 Stenni, B., Buiron, D., Frezzotti, M., Albani, S., Barbante, C., Bard, E., Barnola, J. M., Baroni, M., Baumgartner, M., Bonazza, M., Capron, E., Castellano, E., Chappellaz, J., Delmonte, B., Falourd, S., Genoni, L., Iacumin, P., Jouzel, J., Kipfstuhl, S., Landais, A., Lemieux-Dudon, B., Maggi, V., Masson-Delmotte, V., Mazzola, C., Minster, B., Montagnat, M., Mulvaney, R., Narcisi, B., Oerter, H., Parrenin, F., Petit, J. R., Ritz, C., Scarchilli, C., Schilt, A., Schüpbach, S., Schwander, J., Selmo, E., Severi, M., Stocker, T. F., and Udisti, R.: Expression of the bipolar see-saw in Antarctic climate records during the last
- 500 deglaciation, *Nat. Geosci.*, 4, 46–49, <https://doi.org/10.1038/ngeo1026>, 2011.
- Tian, L., Ritterbusch, F., Gu, J.-Q., Hu, S.-M., Jiang, W., Lu, Z.-T., Wang, D., and Yang, G.-M.: ⁸¹Kr dating at the Guliya ice cap, Tibetan plateau, *Geophys. Res. Lett.*, 46, 6636–6643, <https://doi.org/10.1029/2019GL082464>, 2019.
- Turney, C. S. M., Fogwill, C. J., Golledge, N. R., McKay, N. P., van Sebille, E., Jones, R. T., Etheridge, D., Rubino, M., Thornton, D. P., Davies, S. M., Ramsey, C. B., Thomas, Z. A., Bird, M. I., Munksgaard, N. C., Kohno, M., Woodward, J.,
- 505 Winter, K., Weyrich, L. S., Rootes, C. M., Millman, H., Albert, P. G., Rivera, A., van Ommen, T., Curran, M., Moy, A., Rahmstorf, S., Kawamura, K., Hillenbrand, C.-D., Weber, M. E., Manning, C. J., Young, J., and Cooper, A.: Early last interglacial ocean warming drove substantial ice mass loss from Antarctica, *P. Natl. Acad. Sci. USA.*, 117, 3996–4006, <https://doi.org/10.1073/pnas.1902469117>, 2020.
- Wilhelm, E., Batting, R., and Wilcock, R. J.: Low-pressure solubility of gases in liquid water, *Chem. Rev.*, 77, 219–262, <https://doi.org/10.1021/cr60306a003>, 1977.
- 510 Yan, Y., Bender, M. L., Brook, E. J., Clifford, H. M., Kemeny, P. C., Kurbatov, A. V., Mackay, S., Mayewski, P. A., Ng, J., Severinghaus, J. P., and Higgins, J. A.: Two-million-year-old snapshots of atmospheric gases from Antarctic ice, *Nature*, 574, 663–666, <https://doi.org/10.1038/s41586-019-1692-3>, 2019.



- 515 Yan, Y., Brook, E. J., Kurbatov, A. V., Severinghaus, J. P., and Higgins, J. A.: Ice core evidence for atmospheric oxygen decline since the Mid-Pleistocene transition, *Science Advances*, 7, eabj9341, <https://doi.org/10.1126/sciadv.abj9341>, 2021.
- Yang, J.-W.: Paleoclimate reconstruction from greenhouse gas and borehole temperature of polar ice cores, and study on the origin of greenhouse gas in permafrost ice wedges, PhD thesis, School of Earth and Environmental Sciences, Seoul National University, South Korea, chrome-extension://efaidnbmnnnibpcajpcglclefindmkaj/https://dcollection.snu.ac.kr/public_resource/pdf/000000154664_202503
520 21113749.pdf (last access: 21 March 2025), 2019.
- Yau, A. M., Bender, M. L., Marchant, D. R., and Mackay, S. L.: Geochemical analyses of air from an ancient debris-covered glacier, Antarctica, *Quat. Geochronol.*, 28, 29–39, <https://doi.org/10.1016/j.quageo.2015.03.008>, 2015.
- Zappala, J. C., Baggenstos, D., Gerber, C., Jiang, W., Kennedy, B. M., Lu, Z.-T., Mueller, M. P., Purtschert, R., and Visser, A.: Atmospheric ^{81}Kr as an integrator of cosmic-ray flux on the hundred-thousand-year time scale, *Geophys. Res. Lett.*,
525 47, e2019GL086381, <https://doi.org/10.1029/2019GL086381>, 2020.
- Zekollari, H., Goderis, S., Debaille, V., van Ginneken, M., Gattacceca, J., Team, A., Jull, A. J. T., Lenaerts, J. T. M., Yamaguchi, A., Huybrechts, P., and Claeys, P.: Unravelling the high-altitude Nansen blue ice field meteorite trap (East Antarctica) and implications for regional paleo-conditions, *Geochim. Cosmochim. Ac.*, 248, 289–310, <https://doi.org/10.1016/j.gca.2018.12.035>, 2019.